UCLA

UCLA Previously Published Works

Title

A positivity-preserving numerical method for a thin liquid film on a vertical cylindrical fiber

Permalink

https://escholarship.org/uc/item/5gc0047j

Authors

Kim, Bohyun

Ji, Hangjie

Bertozzi, Andrea L

et al.

Publication Date

2024

DOI

10.1016/j.jcp.2023.112560

Copyright Information

This work is made available under the terms of a Creative Commons Attribution License, available at https://creativecommons.org/licenses/by/4.0/

Peer reviewed

eScholarship.org Powered by the California Digital Library
University of California

Contents lists available at ScienceDirect

Journal of Computational Physics

journal homepage: www.elsevier.com/locate/jcp

A positivity-preserving numerical method for a thin liquid film on a vertical cylindrical fiber

Bohyun Kim[a,*], Hangjie Ji[b], Andrea L. Bertozzi[a,c], Abolfazl Sadeghpour[c], Y. Sungtaek Ju[c]

[a]*Department of Mathematics, University of California, Los Angeles, CA 90095, USA*
[b]*Department of Mathematics, North Carolina State University, Raleigh, NC 27695, USA*
[c]*Department of Mechanical and Aerospace Engineering, University of California, Los Angeles, CA 90095, USA*

ARTICLE INFO

Article history:
Received TBD
Received in final form TBD
Accepted TBD
Available online TBD

Communicated by TBD

ABSTRACT

When a thin liquid film flows down on a vertical fiber, one can observe the complex and captivating interfacial dynamics of an unsteady flow. Such dynamics are applicable in various fluid experiments due to their high surface area-to-volume ratio. Recent studies verified that when the flow undergoes regime transitions, the magnitude of the film thickness changes dramatically, making numerical simulations challenging. In this paper, we present a computationally efficient numerical method that can maintain the positivity of the film thickness as well as conserve the volume of the fluid under the coarse mesh setting. A series of comparisons to experimental data and previously proposed numerical methods supports the validity of our numerical method. We also prove that our method is second-order consistent in space and satisfies the entropy estimate.

© 2023 Elsevier Inc. All rights reserved.

1. Introduction

Fiber coating has complex dynamical properties due to various body forces and the Rayleigh instability from surface tension. An initially uniform flow quickly breaks up into regularly spaced beads, and forms traveling waves in the presence of gravity along the fiber direction [1, 2]. The beaded morphology creates a high surface area-to-volume ratio making it ideal for designing heat and mass transfer devices along the liquid-gas interface [3]. This technique has applications in gas absorption [4, 5, 6], heat exchangers [7, 8], microfluidics [9], and desalination [10]. The practical applications consequently attracted more comprehensive theoretical studies over the last few decades [11, 2, 12, 13, 14, 15, 1, 16]. The fundamental component determining the profile of the thin liquid film on a vertical fiber is surface tension, which has a stabilizing effect on the axial curvatures, and destabilizing effect on the azimuthal curvatures of the interface [17]. In addition, other factors increasing the flow's complexity are the cylindrical geometry

*Corresponding author:
e-mail: bohyunk@math.ucla.edu (Bohyun Kim), hangjie_ji@ncsu.edu (Hangjie Ji), bertozzi@g.ucla.edu (Andrea L. Bertozzi), abolfazlsad@ucla.edu (Abolfazl Sadeghpour), sungtaek.ju@ucla.edu (Y. Sungtaek Ju)

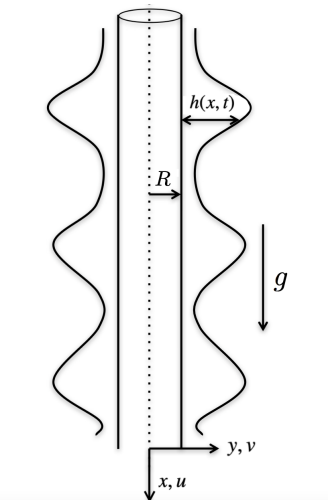

Fig. 1: Illustration of a thin liquid film flowing down a vertical fiber

of the fiber and the gravitational force. Experimentally, interfacial instabilities of the flow have been studied over decades [1, 16]. Kliakhandler et al. experimentally characterized the three distinct regimes of interfacial patterns (*a*)-(*c*) [17]. In this paper, we use the convention by Ji et al. [18] and call (*a*)-(*c*) regimes convective, Rayleigh-Plateau, and isolated droplet regimes. The convective regime, observed when the flow rate is high, corresponds to the flow profile where irregular droplets collide with each other. The Rayleigh-Plateau regime corresponds to the flow profile where beaded traveling waves propagate nearly constantly. The isolated droplet regime, observed when the flow rate is low, corresponds to the flow profile where small wavy patterns follow well-separated large droplets. The distinct dynamics of each regime and its transition is extensively studied, both theoretically and experimentally [16, 19, 2, 20, 18, 21].

In this paper, we consider reduced-order models of the Navier-Stokes equations incorporating linear and nonlinear effects of the flow. Li and Chao [22] summarize a few notable methods: the gradient expansion method [23, 24, 25, 18], the integral method [26, 27], the weighted residual method [14, 20, 13], and the energy integral method [28]. The models are often classified according to the size of the Reynolds number. For the low Reynolds number cases, the flow profile is approximated by the Stokes equations combined with the lubrication approximation [18, 24]. For moderate Reynolds number cases, one incorporates inertial terms in the governing equation using the weighted residual boundary integral method [14, 13]. Many of the models are verified against the experimental data [14, 13]. For example, a recent study by Ji et al. shows a good agreement with experimental data by correctly predicting bead velocities, flow profiles, and regime transition bifurcation [18].

A major challenge is that fiber coating equations are extremely difficult to solve both numerically and analytically. They are typically fourth-order degenerate nonlinear parabolic equations due to the surface tension in the dynamics. We consider the following model from [18].

$$\begin{aligned} &\frac{\partial}{\partial t}\left(h+\frac{\alpha}{2}h^2\right)+\frac{\partial}{\partial x}\mathcal{M}(h)+\frac{\partial}{\partial x}\left[\mathcal{M}(h)\frac{\partial p}{\partial x}\right]=0,\\ &\mathcal{M}(h)=O(h^n),\ \ p=\frac{\partial^2 h}{\partial x^2}-\mathcal{Z}(h). \end{aligned} \tag{1}$$

Equation (1) is an evolution equation of the film thickness $h(x,t)$. From left to right,

- $\frac{\partial}{\partial t}(h+\frac{\alpha}{2}h^2)$ denotes the mass change over time where $\alpha = \mathcal{H}/\mathcal{R} \geq 0$ is the aspect ratio between the characteristic length scale of film thickness $\mathcal{H}$ to the fiber radius R.
- $\mathcal{M}(h)$ is often referred to as the mobility function that describes the hydrodynamic interactions of the transverse waves. Many times, $\mathcal{M}(h) = O(h^n)$. For example, setting $\mathcal{M}(h)$ to $\mathcal{M}(h) = h^3$ corresponds to the no-slip

boundary condition, and setting $\mathcal{M}(h)$ to $h^3 + \beta h^n$ for $n \in (0, 3)$ corresponds to various Navier-slip conditions. The smoothness of $\mathcal{M}(h)$ near $h = 0$ determines the qualitative behavior of solutions at zero.

- The pressure p consists of two terms - the linearized curvature $\frac{\partial^2 h}{\partial x^2}$, representing the streamwise surface tension, and the $\mathcal{Z}(h)$, representing other nonlinear pressure effects. $\mathcal{Z}(h)$ often contains a destabilizing surface tension term that arises from the azimuthal curvature but can also include other terms.

Equation (1) is considered state of the art for this problem because it quantitatively agrees with bead velocities, flow profiles, and regime transition bifurcations as compared to experiments. Previously, the model by Kliakhandler et al. [17] incorporated fully nonlinear curvature to capture the qualitative behavior of the Rayleigh-Plateau and isolated droplet regime. Nevertheless, this model overestimated the beads' velocity by 40%. Craster & Matar's model [24] revisited this idea and presented an asymptotic model describing Rayleigh-Plateau and isolated droplet regime but again overestimated the bead velocity. Their model also identified the Rayleigh-Plateau regime to be transient rather than a stationary state. Duprat et al. [29], and Smolka et al. [30] further studied regime transitions but predicting the regime transitions remained challenging. Ji et al.'s film stabilization model (FSM) [18] improved the preceeding models by incorporating a film stabilization term among generalized pressure terms. This stabilization term was inspired by the attractive part of the long-range apolar van der Waals forces, which are carefully studied for the well-wetting liquids [31, 32]. One can see that simulating such complex models is a delicate procedure. Thus, it is vital to have a robust numerical method for simulating complex spatiotemporal dynamics to predict flow profiles and regime transitions.

The degeneracy of the mobility function $\mathcal{M}(h)$ and the complex nonlinear pressure terms $\mathcal{Z}(h)$ are two hurdles one needs to clear to construct a robust numerical method. First, the degeneracy of the mobility function presents a substantial challenge in numerically solving equation (1) since the solution may lose regularity as $h \to 0$. Second, the nonlinear term $\mathcal{Z}(h)$ in pressure p complicates the problem further since it is often relatively large in magnitude as $h \to 0$. As a result, the numerical method can suffer from instabilities as $h \to 0$. Therefore, keeping h positive is not only crucial for the solution to be physically meaningful but also important for the solution to be accurate. Fortunately, we found similarities between equation (1) and many lubrication-type equations and realized we could view equation (1) as a variant of a lubrication-type equation with generalized pressure [33, 34].

$$\frac{\partial h}{\partial t} + \frac{\partial}{\partial x}\left(\mathcal{M}(h)\frac{\partial p}{\partial x}\right) = 0 \quad p = \frac{\partial^2 h}{\partial x^2} - \mathcal{Z}(h) \quad \text{where} \quad f(h) \sim h^n \quad \text{as} \quad h \to 0. \tag{2}$$

One may see that setting $\alpha = 0$ and $\frac{\partial}{\partial x}\mathcal{M}(h) = 0$ in equation (1) results in equation (2). Setting $\alpha = 0$ would mean neglecting the effect of the fiber, and $\frac{\partial}{\partial x}\mathcal{M}(h) = 0$ would mean neglecting the advection effect by liquid traveling downward. Such experimental and theoretical settings are discussed in various studies devoted to the lubrication theory so that we can take advantage of them [35, 36, 37, 33, 38]. We know the solution of (2) is smooth whenever the solution is positive but typically loses its regularity as the solution $h \to 0$ due to the degeneracy of the equation [39, 40]. We also know that the nonlinear pressure terms often introduce a large numerical instability as $h \to 0$, making it challenging to maintain the positive numerical solution [33, 38]. Examples of fiber coating problems include $\mathcal{Z}(h) = -(\alpha/\epsilon)^2 h$ in [41], assuming the thickness of the film is much smaller than the fiber radius ($\mathcal{H} \ll R$). Craster & Matar [24] used $\mathcal{Z}(h) = \frac{\alpha}{\eta(1+\alpha h)}$, assuming the film thickness comparable to the fiber radius ($\alpha = O(1)$). Ji et al. [18] used that $\mathcal{Z}(h) = \frac{\alpha}{\eta(1+\alpha h)} - \frac{A}{h^3}$. In both the Craster & Matar model and Ji et al. model, we can expect numerical challenges when h is small. Indeed, we show in section 4 that the numerical method used in [18] can generate a false singularity of the form $h \to 0$ when the spatial grid size is underresolved. In other words, although the analytical solution of (1) is positive everywhere, the solution produced by a naive numerical method can produce negative values within some range of the solution when the grid size is underresolved. Such numerical methods can be quite difficult to extend to higher dimensions where grid refinement is computationally expensive. We also show that the negativity further prevents calculating the solution after the singularity. Thus, it is desirable to have a positivity-preserving numerical method that can perform well at different grid resolutions without spurious numerical singularities.

Constructing positivity preserving methods for partial differential equations (PDEs) is addressed in a wealth of literature yet most of them are limited to the first or second-order equations [42, 43, 44, 45]. Equations above the second order have no maximum or comparison principles, and higher-order spatial derivatives make the numerical system extremely stiff. Numerical methods for fourth or higher-order equations with positivity-preserving properties

have received far less attention. Early works include [46, 47, 48, 38] and make use of entropy estimates to prove positivity. Some of the recent approaches use cut-off, or Lagrange multiplier methods which have a limitation in conserving mass or maintaining smoothness [49, 50]. Here we introduce a convex-splitting method that preserves physical quantities like energy, entropy, and mass [51, 52, 53, 33] which treats the stabilizing stiffest terms implicitly and the destabilizing terms explicitly. A few methods are unconditionally stable [54, 55] which include the scalar auxiliary variable (SAV) method by Huang et al. [56]. The applications of these methods are to solve Cahn-Hilliard or Hele-Shaw cell-type equations.

This paper presents a positivity-preserving numerical scheme that works on a general family of lubrication-type equations on cylindrical geometries. Positivity-preserving numerical methods have not been studied in the context of fiber coating, especially in the regime that is most relevant to physical experiments. The structure of the paper follows. In section 2, we prove properties that the PDE (1) holds and discuss how the PDE imparts such properties to our numerical methods. In section 3, we introduce our numerical method and the state of art method in [18]. In section 4, we present proofs on the positivity and the consistency of our method. In section 5, we compare numerical simulations of our method to simulations of the state of the art method and experimental data. In section 6, we conclude our paper with a few remarks.

2. Properties of the partial differential equation

This section investigates two essential properties of the continuous fiber coating equation (1). We ensure that our numerical method preserves the discrete equivalent of the properties. We consider the following initial-boundary value problem:

$$(P)\begin{cases} \dfrac{\partial}{\partial t}\left(h+\dfrac{\alpha}{2}h^2\right)+\dfrac{\partial}{\partial x}\left[\mathcal{M}(h)\left(1+\dfrac{\partial p}{\partial x}\right)\right]=0 \text{ in } L_T=(0,L)\times(0,T)\subset\mathbb{R}^2,\\ p=\dfrac{\partial^2 h}{\partial x^2}-\mathcal{Z}_+(h)-\mathcal{Z}_-(h),\\ [0,L]-\text{periodic boundary conditions},\\ h(x,0)=h_0(x)>0. \end{cases}$$

The main difference from previous equation (1) is that we split $\mathcal{Z}(h)$ into two parts: $\mathcal{Z}_+(h)$ and $\mathcal{Z}_-(h)$, where $\mathcal{Z}'_+(h)\geq 0$ and $\mathcal{Z}'_-(h)\leq 0$. Such splittings are not generally unique but useful in the design of stable numerical schemes. An example is discussed in Section 4. We assume periodic boundary conditions for simplicity and a positive initial condition to match the physical setting.

Here we assume that a smooth positive solution exists to the problem (P). The existence of a solution to problems such as (P) has been studied in depth [57, 58, 21]. The general procedure is like this. First, one applies a regularization technique to a problem (P) to overcome the degeneracy and make the problem uniformly parabolic. The boundary condition can be extended to the whole line using a proper continuation technique such as the one suggested in [59]. The well-known parabolic Schauder estimates [60, 59, 61] guarantees a unique solution in a small time interval say, $L_\tau=(0,L)\times(0,\tau)$. In the end, the limit of the regularized solution results is a smooth, positive solution. We direct our readers to [57, 21] for the full derivation. We believe a similar derivation is possible through the canonical approach although continuation of solutions past the initial small time interval requires a priori bounds on certain norms. A full discussion of this problem is beyond the scope of this paper.

The key idea of developing a positivity-preserving numerical method is to formulate an entropy estimate for the continuous problem (P). Such an estimate guarantees the positivity of solutions in the continuous setting. Therefore, one may yield a positivity-preserving numerical method by constructing a numerical method that satisfies the discrete equivalent of the entropy estimate. For our problem (P), we define entropy $G(h)$ so that its derivative satisfies

$$G'(h)=(1+\alpha h)\int_A^h \frac{1}{\mathcal{M}(s)}\,ds, \text{ for some fixed } A>0.$$

We note that the numerical methods to be developed in Section 3 do not explicitly involve the constant $A>0$, and we will show that the analytical proof of the algorithm in sections 2 and **??** does not depend on any particular choice of A. We claim that solutions to the problem (P) satisfy conservation of mass and an entropy estimate.

Proposition 2.1. *Suppose that there exists a solution $h \in C^4(L_T)$ of (P), where $L_T = [0, L) \times [0, T)$. Suppose we further assume*

$$\mathcal{M}(h) = O(h^n), \mathcal{M}(h) \geq 0$$
$$\mathcal{Z}_+, \mathcal{Z}_- \in C^2(\mathbb{R}^+), \quad \text{and} \quad \mathcal{Z}'_+(h) \geq 0, \mathcal{Z}'_-(h) \leq 0.$$

Then, the solution h satisfies the following two properties;

$$(I) \int_0^L h(x,T) + \frac{\alpha}{2}h^2(x,T)\,dx = \int_0^L h(x,0) + \frac{\alpha}{2}h^2(x,0)\,dx \ (\textit{conservation of mass}),$$
$$(II) \int_0^L G(h(x,T))\,dx \leq \int_0^L G(h(x,0))\,dx + \int_{L_T} \left(\frac{\mathcal{Z}_-(h)}{2}\right)^2 dxdt, \ \textit{for some fixed } A > 0. \ (\textit{entropy estimate})$$

Proof. The conservation of mass (I) is achieved by integrating the problem (P) on L_T.

$$\int_{L_T} \frac{\partial}{\partial t}\left(h + \frac{\alpha}{2}h^2\right)dxdt = -\int_{L_T} \frac{\partial}{\partial x}\left[\mathcal{M}(h)\left(1 + \frac{\partial p}{\partial x}\right)\right]dxdt$$
$$\implies \int_0^L \left(h(x,T) + \frac{\alpha}{2}h^2(x,T)\right)dxdt - \int_0^L \left(h(x,0) + \frac{\alpha}{2}h^2(x,0)\right)dxdt = 0$$

Note that the periodic boundary condition removes the complex expression surrounded by $\frac{\partial}{\partial x}[...]$.

The entropy estimate (II) is achieved by directly calculating the time derivative of $G(h)$.

$$\begin{aligned}
\frac{d}{dt}\int_0^L G(h)dx &= \int_0^L G'(h)h_t dx \\
&= \int_0^L \left\{(1 + \alpha h)h_t \int_A^h \frac{1}{\mathcal{M}(s)}ds\right\}dx \\
&= -\int_0^L \left\{\frac{\partial}{\partial x}\left[\mathcal{M}(h)\left(1 + \frac{\partial p}{\partial x}\right)\right]\int_A^h \frac{1}{\mathcal{M}(s)}ds\right\}dx \\
&= \int_0^L h_x\left(1 + \frac{\partial p}{\partial x}\right)dx.
\end{aligned}$$

The equalities are justified by the integration by parts. Note that the periodic boundary plays a crucial role in simplifying expressions on the boundary. We use the definition $p = h_{xx} - \mathcal{Z}(h) = h_{xx} - \mathcal{Z}_+(h) - \mathcal{Z}_-(h)$ to continue our calculation.

$$\begin{aligned}
\frac{d}{dt}\int_0^L G(h)dx &= \int_0^L h_x dx + \int_0^L h_x \frac{\partial}{\partial x}\left(h_{xx} - \mathcal{Z}(h)\right)dx \\
&= -\int_0^L h_{xx}^2 + \int_0^L h_{xx}\mathcal{Z}_-(h)dx - \int_0^L h_x^2\mathcal{Z}'_+(h)dx \\
&= -\int_0^L \left(h_{xx} - \frac{Z_-(u_i)}{2}\right)^2 dx + \int_0^L \left(\frac{Z_-(u_i)}{2}\right)^2 dx - \int_0^L h_x^2\mathcal{Z}'_+(h)dx \\
&\leq -\int_0^L \left(h_{xx} - \frac{Z_-(u_i)}{2}\right)^2 dx + \int_0^L \left(\frac{Z_-(u_i)}{2}\right)^2 dx.
\end{aligned}$$

Again, the periodic boundary is crucial in eliminating $\int_0^L h_x dx$ in the first line. We use the Completing the Square trick in the third line to simplify the expression. We get the inequality in the last line because $\mathcal{Z}'_+(h) \geq 0$. Integrating the consequent expression over time gives us

$$\int_0^L G(h(x,T))\,dx + \int_{L_T}\left(h_{xx} - \frac{\mathcal{Z}_-(h)}{2}\right)^2 dxdt \le \int_0^L G(h(x,0))\,dx + \int_{L_T}\left(\frac{\mathcal{Z}_-(h)}{2}\right)^2 dxdt.$$

Finally, one can drop the second term on the left side of the inequality since it is nonnegative. □

The above properties allow us to create a positivity-preserving numerical method due to the entropy estimate. Lubrication-type equations are well-known to satisfy entropy dissipating properties. Bernis et al. recognized the significance of the entropy dissipation property in third-order or higher degenerate parabolic equations and used it to prove the nonnegativity of weak solutions [57] with sufficiently high degeneracy in one space dimension. They also proved that the solution is unique and strictly positive if the mobility order $n \ge 4$. Following their work, several articles regarding lubrication-type equations discussed the importance of entropy estimates in numerical and analytical contexts [39, 62, 47, 46, 48, 33]. These ideas have largely been lacking in the fiber coating problem, except for the generalized entropy analysis done by Ji et al. [21], which proves the existence of a nonnegative weak solution of a fiber-coating model with fully nonlinear curvature terms. In this paper, we use these ideas to develop a positivity-preserving numerical solution.

3. Positivity-preserving Finite difference method

In this section, we present a positivity-preserving finite difference method, the Bounded Entropy Method (BEM), and compare it to the current state of the art method General Method (GM) used in fiber coating models [18]. Our method is second-order accurate in space and first-order accurate in time while preserving the positivity of a numerical solution at each time step. Our method is motivated by prior work by Zhornitskaya et al. [47] and Grun et al. [33] for a simple lubrication model without the geometry and physics of fiber coating. Before introducing our method, we define the following notation.

Notation. *Suppose we divide our domain* $[0, L]$ *into* N *equally spaced grids of size* $\Delta x = L/N$. *Assume* $u_i(t)$ *to be a solution of a numerical method at time* t *and the* i*-th grid. Define the forward difference in space and the backward difference in space as*

$$u_{i,x} = \frac{u_{i+1}(t) - u_i(t)}{\Delta x}, \quad u_{i,\bar{x}} = \frac{u_i(t) - u_{i-1}(t)}{\Delta x}.$$

Respectively, higher-order differences in space can be defined as

$$u_{i,\bar{x}x} = \frac{u_{i+1,\bar{x}} - u_{i,\bar{x}}}{\Delta x}, \quad u_{i,\bar{x}x\bar{x}} = \frac{u_{i,\bar{x}x} - u_{i-1,\bar{x}x}}{\Delta x}.$$

We define our discrete mobility function to satisfy the following criteria.

Definition 3.1 (Discretization of Mobility)**.** *The mobility term* $\mathcal{M}(s)$ *in the problem* (P) *is discretized to satisfy the following criteria [47].*

(a) $m(s, s) = \mathcal{M}(s)$,

(b) $m(s_1, s_2) = m(s_2, s_1)$,

(c) $m(s_1, s_2) \in C^4((0,\infty)\times(0,\infty)) \cap C([0,\infty]\times[0,\infty])$,

(d) $\forall \delta > 0$, *there exists* $\gamma > 0$ *such that* $s_1, s_2 > \delta \implies m(s_1, s_2) \ge \gamma > 0$.

Note that the discretized mobility $m(s_1, s_2)$ is symmetric and continuously differentiable everywhere except at 0. $m(s_1, s_2)$ is continuous at 0 but does not have to be differentiable. Condition (d) allows the $m(s_1, s_2)$ to be degenerate if one of the arguments $h \to 0$ but guarantees positivity if both of the arguments are greater than 0. We define our positivity-preserving finite difference method BEM to satisfy the above definition.

Bounded Entropy Method (BEM). *The finite difference discretization of the problem* (P) *with continuous time is written by the following equations.*

$$\begin{aligned}
&(1+\alpha u_i)\frac{du_i}{dt} + [m(u_{i-1},u_i)(1+p_{i,\bar{x}})]_x = 0, \quad p_i = u_{i,\bar{x}x} - \mathcal{Z}_+(u_i) - \mathcal{Z}_-(u_i),\\
&u_i(0) = u_0(i\Delta x),\ i = 0,1,2\cdots N,\\
&m(s_1,s_2) = \begin{cases} \mathcal{M}(s_1) & \text{if } s_1 = s_2\\ (s_2-s_1)/\int_{s_1}^{s_2}\frac{1}{\mathcal{M}(s)}ds & \text{if } s_1 \neq s_2. \end{cases}
\end{aligned} \tag{3}$$

In section 4, we show that the above discretization of $\mathcal{M}(h)$ guarantees a discrete equivalent of the conservation of mass (I) and the entropy estimate (II). We can also write the numerical method of Ji et al. [18] as the following, which we refer to as Generic Method (GM).

Generic Method (GM). *The finite difference discretization of the problem* (P) *with continuous time is written by the following equations.*

$$\begin{aligned}
&(1+\alpha u_i)\frac{du_i}{dt} + [m(u_{i-1},u_i)(1+p_{i,\bar{x}})]_x = 0, \quad p_i = u_{i,\bar{x}x} - \mathcal{Z}_+(u_i) - \mathcal{Z}_-(u_i),\\
&u_i(0) = u_0(i\Delta x),\ i = 0,1,2\cdots N,
\end{aligned} \tag{4}$$

where $m(s_1,s_2)$ *satisfies Definition 3.1.*

For example, one can use $m(s_1,s_2) = \mathcal{M}(0.5(s_1+s_2))$ and $m(s_1,s_2) = 0.5(\mathcal{M}(s_1)+\mathcal{M}(s_2))$ for GM. Note that $m(s_1,s_2)$ in BEM and GM is center-difference, allowing the numerical method to conserve flux at each time step. Together with second-order consistency, both numerical methods are "shock capturing," which is a desirable property to have in conservation law type of equations [63]. In the following section, we show that BEM satisfies the conservation of mass and entropy estimate, which allows us to prove the positivity of the numerical method.

4. Positivity of Numerical solutions

In the previous section, we claim that discretizing $m(s_1,s_2)$ using Definition 3.1 allows us to preserve the conservation of mass and the entropy estimates discussed in section 2. In this section, we show how such a discretization preserves the positivity of BEM. Specifically, we prove discrete conservation of mass and the entropy estimate in Proposition 4.1 and show the positivity preserving property of BEM in Theorem 4.1. Our method is inherently more complex than entropy dissipating schemes for traditional lubrication-type equations because of three reasons. First, the time derivative of (1) involves the geometry of the cylindrical fiber $\frac{\alpha}{2}h^2$. Second, a nonlinear advection $\frac{\partial}{\partial x}\mathcal{M}(h)$ is incorporated. Lastly, nonlinear pressure p entails a destabilizing azimuthal curvature $\frac{\alpha}{\eta(1+\alpha h)}$. The coupled entropy estimate expression in Proposition 2.1 is consequently more complicated than "entropy dissipation", which is the case for the conventional lubrication-type equations. We prove the discrete analog of Proposition 2.1.

Proposition 4.1. *Suppose* $u_i(t)$ *is a solution of the BEM* (3) *at time* t *and* i*-th grid in space. Suppose we further assume*

$$\begin{aligned}
&\mathcal{M}(h) = O(h^n), \mathcal{M}(h) \geq 0\\
&\mathcal{Z}_+, \mathcal{Z}_- \in C^2(\mathbb{R}^+), \quad \text{and} \quad \mathcal{Z}'_+(h) \geq 0, \mathcal{Z}'_-(h) \leq 0.
\end{aligned}$$

We remind the readers that the derivative of entropy $G(h)$ *satisfies*

$$G'(h) = (1+\alpha h)\int_A^h \frac{1}{\mathcal{M}(s)}\,ds, \ \text{for some fixed } A > 0.$$

Then, $u_i(t)$ satisfies the following two properties given $T > 0$;

$$(I)\ \sum_i \left(u_i(T) + \frac{\alpha}{2}u_i(T)^2\right)\Delta x = \sum_i \left(u_i(0) + \frac{\alpha}{2}u_i(0)^2\right)\Delta x \ (\textit{Discrete conservation of mass}),$$

$$(II)\ \sum_i G(u_i(T))\Delta x \le \sum_i G(u_i(0))\Delta x + \int_0^T \sum_i \left(\frac{\mathcal{Z}_-(u_i(s))}{2}\right)^2 \Delta x ds \ (\textit{Discrete entropy estimate}).$$

Proof. The proof of the statements is very similar to the proof of Proposition 2.1. The only difference is that we multiply by Δx and sum over $i = 0, 1, 2... N-1$ instead of integrating over space. Discrete conservation of mass (I) is achieved by integrating the first line of (3) by time and summing over $i = 0, 1, 2... N-1$.

$$\int_0^T \sum_i (1+\alpha u_i)\frac{du_i}{dt}\Delta x = -\int_0^T \sum_i [m(u_{i-1}, u_i)(1 + p_{i,\bar{x}})]_x \Delta x.$$
$$\implies \sum_i \left(u_i(T) + \frac{\alpha}{2}u_i(T)^2\right)\Delta x - \sum_i \left(u_i(0) + \frac{\alpha}{2}u_i(0)^2\right)\Delta x = 0.$$

As we saw in the continuous case, the periodic boundary condition removes the expression surrounded by $[...]_x$.

Discrete entropy estimate (II) is achieved by direct calculation.

$$\begin{aligned}
\frac{d}{dt}\sum_i G(u_i)\Delta x &= \sum_i G'(u_i)\frac{du_i}{dt}\Delta x \\
&= -\sum_i \int_A^{u_i} \frac{1}{\mathcal{M}(s)} ds [a(u_{i-1}, u_i)(1 + p_{i,\bar{x}})]_x \Delta x \\
&= \sum_i \frac{1}{\Delta x}\left(\int_{u_{i-1}}^{u_i} \frac{1}{\mathcal{M}(s)} ds\right) a(u_{i-1}, u_i)(1 + p_{i,\bar{x}})\Delta x \\
&= \sum_i u_{i,\bar{x}}(1 + p_{i,\bar{x}})\Delta x \\
&= \sum_i \left\{-(u_{i,\bar{x}x})^2 - u_{i,\bar{x}}[\mathcal{Z}'_+(u_i)]_{\bar{x}} + u_{i,\bar{x}x}\mathcal{Z}_-(u_i)\right\}\Delta x \\
&\le -\sum_i \left(u_{i,\bar{x}x} - \frac{\mathcal{Z}_-(u_i)}{2}\right)^2 \Delta x + \sum_i \left(\frac{\mathcal{Z}_-(u_i)}{2}\right)^2 \Delta x.
\end{aligned}$$

Until the 4th line, the equalities are justified by integration by parts. Note that the periodic boundary plays a crucial role in simplifying expressions on the boundary and eliminating $\sum_i u_{i,\bar{x}}\Delta x$ in the 4th line. We obtain the inequality in the last line after using Completing the Square trick and using the fact that $\mathcal{Z}'_+ \ge 0$. From the inequality, one integrates over time from 0 to T.

$$\sum_i G(u_i(T))\Delta x + \int_0^T \sum_i \left(u_{i,\bar{x}x}(s) - \frac{\mathcal{Z}_-(u_i(s))}{2}\right)^2 \Delta x ds \le \sum_i G(u_i(0))\Delta x + \int_0^t \sum_i \left(\frac{\mathcal{Z}_-(u_i(s))}{2}\right)^2 \Delta x ds$$

Finally, one can drop the second term on the left side since it is nonnegative and the desired entropy estimate is achieved. □

We have two versions of theorems on the positivity: (a) a priori bound - depending on Δx and (b) a posteriori bound assuming a uniform Lipschitz condition on the numerical solution. We note that the solution is observed to have a uniform Lipschitz bound in all of our numerical simulations. Thus, the uniform Lipschitz assumption is logically coherent. We leave proving the smoothness of PDE, such as establishing a uniform Lipschitz bound, as future work.

Theorem 4.1. *(Positivity of BEM) Suppose we have the same assumptions as Proposition 4.1. We further assume that* $(Z_-(s))^2 \le C_1$ *for any* $s \ge 0$ *and the initial data* $u_i(0) > 0$*. Then, the solution of BEM at time* $T > 0$*,* $u_i(T)$*, satisfies the following conditions;*

(a) if $n \ge 2$*, there exists* δ *such that* $u_i(T) \ge \delta(\Delta x) > 0$ *for all* i*,*

(b) if $n > 2$ *and* $u_i(t)$ *is uniformly Lipchitz on* $[0, T]$*, i.e.* $|u_i(s) - u_j(s)| \le C_L|(i-j)\Delta x|$*,* $\forall i, j$*,* $\forall 0 \le s \le T$*, for some* $C_L > 0$*, there is a posteriori lower bound* δ *such that* $u_i(T) \ge \delta > 0$*. In this case,* δ *is independent of* Δx*.*

Proof. Notice that we assume that $\mathcal{M}(h) = O(h^n)$ and consider cases where $n \ge 2$. Thus, for simplicity, we take $\mathcal{M}(h) = h^n$ throughout the proof. More general cases can be proved as in similar fashions. Let us first prove the statement (a). The given assumptions allow us to use the discrete entropy estimate (II) from Proposition 4.1. First, we claim that $\sum_i G(u_i(T))\Delta x \le C$ for some fixed constant C. We express the entropy function $G(h)$ as

$$G(h) = \begin{cases} -\ln h + O(h) + O(1) & \text{if } n = 2, \\ \frac{1}{(n-1)(n-2)} h^{-(n-2)} + O(h^{3-n}) + O(1) & \text{if } 2 < n < 3, \\ \frac{1}{2h} - \frac{\alpha}{2} \ln h + O(h) + O(1) & \text{if } n = 3, \\ \frac{1}{(n-1)(n-2)} h^{-(n-2)} + \frac{\alpha}{(n-1)(n-3)} h^{-(n-3)} + O(h) + O(1) & \text{if } n > 3, \end{cases}$$

Here, the choice of A only affects the coefficients of the higher order terms but not the leading order term. Because we have fixed positive initial data $u_i(0)$, each $G(u_i(0))$ is well defined. This leads us to conclude

$$\sum_i G(u_i(0))\Delta x \le C_0.$$

We also have the assumption $(Z_-(u_i(s)))^2 \le C_1$ so

$$\int_0^T \sum_i \left(\frac{\mathcal{Z}_-(u_i(s))}{2} \right)^2 \Delta x ds \le C_2 T$$

Hence, we get

$$\sum_i G(u_i(T))\Delta x \le \sum_i G(u_i(0))\Delta x + \int_0^T \sum_i \left(\frac{\mathcal{Z}_-(u_i(s))}{2} \right)^2 \Delta x ds \le C_0 + C_2 T \le C.$$

Next, we show that $\delta(T) = \min_i u_i(T) \ge 0$ using the boundedness of $\sum_i G(u_i(T))\Delta x$. Note that

$$G(\delta) = \begin{cases} -\ln \delta + O(\delta) + O(1) & \text{if } n = 2, \\ \frac{1}{(n-1)(n-2)} \delta^{-(n-2)} + O(\delta^{3-n}) + O(1) & \text{if } 2 < n < 3, \\ \frac{1}{2\delta} - \frac{\alpha}{2} \ln \delta + O(\delta) + O(1) & \text{if } n = 3, \\ \frac{1}{(n-1)(n-2)} \delta^{-(n-2)} + \frac{\alpha}{(n-1)(n-3)} \delta^{-(n-3)} + O(\delta) + O(1) & \text{if } n > 3, \end{cases}$$

Notice that all the leading order terms of $G(\delta)$ is positive as $\delta \to 0$, up to constant differences. Thus, $\delta \to 0$ implies $G(\delta) \to +\infty$, which contradicts $\sum_i G(u_i(T))\Delta x \le C$. Hence, we achieve $\min_i u_i(T) = \delta > 0$.

To prove (b), we use $\sum_i G(u_i(T))\Delta x \le C$ as well. From part (a), we have nonnegativity of $u_i(T)$ so

$$G(u_i(T)) = \int_B^{u_i} (1 + \alpha v) \int_A^v \frac{1}{\mathcal{M}(s)} ds dv + O(1) \ge \int_B^{u_i} \int_A^v \frac{1}{\mathcal{M}(s)} ds dv + O(1), \text{ for some } B > 0.$$

Therefore,

$$C \ge \sum_i G(u_i(T))\Delta x \ge \sum_i \int_B^{u_i} \int_A^v \frac{1}{\mathcal{M}(s)} ds dv \Delta x + O(1) \ge \sum_i \int_B^{u_i} \int_A^v \frac{1}{s^n} ds dv \Delta x + O(1) = \sum_i u^{2-n} \Delta x + O(1).$$

Suppose $\delta(T) = \min_i u_i(T)$ occurs at i^*. Due to the uniform Lipschitzness, $u_i \le \delta + C_L|(i^* - i)\Delta x|$, $\forall i$.

$$\tilde{C} \ge \sum_i \frac{1}{u_i^{n-2}}\Delta x \ge \sum_i \frac{\Delta x}{(\delta + C_L|(i - i^*)\Delta x|)^{n-2}} \ge \sum_i \frac{\Delta x}{(\delta + C_L(i\Delta x))^{n-2}}$$
$$\ge \int_0^L \frac{dx}{(\delta + C_L x)^{n-2}} \ge \frac{1}{C_L\delta^{n-1}} \int_0^{LC_L/\delta} \frac{ds}{(1+s)^{n-2}}$$

If $\frac{LC_L}{\delta} \le 1 \implies \delta \ge LC_L$ so we have lower bound for δ independent of Δx. In the case when $\frac{LC_L}{\delta} \ge 1$,

$$\tilde{C} \ge \frac{1}{C_L\delta^{n-1}} \int_0^1 \frac{ds}{(1+s)^n} = \frac{C'}{\delta^{n-1}}.$$
$$\implies \delta \ge \left(\frac{C'}{\tilde{C}}\right)^{1/n-1}.$$

□

Corollary 4.2. *Numerical solutions of Craster-Matar model [24] and Film Stabilization Model (FSM) [18] are positivity preserving if we use the BEM.*

Proof. For both cases, the same mobility function $\mathcal{M}(h)$ is used but different $\mathcal{Z}(h)$ are used.

$$\mathcal{M}(h) = \frac{h^3}{3}\frac{\phi(\alpha h)}{\phi(\alpha)} + \frac{h^2(\alpha h + 2)^2\lambda}{4\phi(\alpha)},$$
$$\phi(x) = \frac{3}{16x^3}\left[(1+x)^4(4\ln(1+x) - 3) + 4(1+x)^2 - 1\right],$$
$$\mathcal{Z}_{CM}(h) = \mathcal{Z}_{CM-}(h) = \frac{\alpha}{\eta(1+\alpha h)},$$
$$\mathcal{Z}_{FSM}(h) = \mathcal{Z}_{FSM+} + \mathcal{Z}_{FSM-} = -\frac{A_H}{h^3} + \frac{\alpha}{\eta(1+\alpha h)}.$$

We prove that the assumptions for Theorem 4.1 are satisfied by showing that $\mathcal{M}(h) = O(h^2)$ as $h \to 0$ and $(\mathcal{Z}_-(s))^2 \le \left(\frac{\alpha}{\eta}\right)^2$. To simplify the calculation, let $y = \alpha h$. Then,

$$\frac{h^3\phi(\alpha h)}{3\phi(\alpha)} = \frac{1}{16\alpha^3\phi(\alpha)}\left[(y+1)^4(4\ln(y+1) - 3) + 4(y+1)^2 - 1 + 4\lambda\alpha y^2(y+2)^2\right]$$
$$= \frac{1}{C}\left[A_4y^4 + A_3y^3 + A_2y^2 + A_1y + A_0\right],$$

where

$$A_4 = 4\alpha\lambda + 4\ln(y+1) - 3,\ A_3 = 16\alpha\lambda + 16\ln(y+1) - 12,\ A_2 = 16\alpha\lambda + 24\ln(y+1) - 14,$$
$$A_1 = 16\ln(y+1) - 4,\ A_0 = 4\ln(y+1).$$

As $y \to 0$, $ln(y+1) = O(y)$. Thus,

$$\frac{h^3\phi(\alpha h)}{3\phi(\alpha)} = O(y^2) + \frac{1}{C}[A_1y + A_0] = O(y^2) + 16y^2 - 4y + 4y = O(y^2) = O(s^2).$$

Finally, for any $s \ge 0$,

$$\mathcal{Z}_-(s) = \frac{\alpha}{\eta(1+\alpha s)} \le \frac{\alpha}{\eta}.$$

To finish the proof, we apply Theorem 4.1. and see that the numerical solutions of both Craster-Matar Model and FSM are positive. □

Theorem 4.3 (Consistency)**.** *GM and BEM are second-order consistent in space. That is, given a smooth solution $u(x,t)$ of the problem (P), a local truncation error $\tau_i(t)$ is $O(\Delta x^2)$. Where*

$$\tau_i(t) = (1+\alpha u_i)u_{i,t} + [m(u_{i-1},u_i)(1+p_{i,\bar{x}})]_x.$$

Proof. Let us denote $u_i = u(i\Delta x, t)$ to simplify the notation. First, note that both GM and BEM have very similar formulations and satisfy Definition 3.1. Thus, we can use an approach similar to [47]. After Taylor expansion,

$$\begin{aligned} m(s_1,s_2) &= m(s+\Delta s, s-\Delta s) = m(s,s) + \frac{\partial m}{\partial s_1}(s,s)\Delta s - \frac{\partial m}{\partial s_2}(s,s)\Delta s + \beta(s)\Delta s^2 + O(\Delta s^2) \\ &= \mathcal{M}(s) + \beta(s)\Delta s^2 + O(\Delta s^2), \end{aligned}$$

where $s = \frac{s_1+s_2}{2}, \Delta s = \frac{s_1-s_2}{2}$, and

$$\beta(s) = \frac{1}{2}\left(\frac{\partial^2 m(s,s)}{\partial s_1^2} - 2\frac{\partial^2 m(s,s)}{\partial s_1 \partial s_2} + \frac{\partial^2 m(s,s)}{\partial s_2^2}\right)$$

We canceled out $O(\Delta s)$ terms by using the symmetry of $m(s_1,s_2)$, according to (b) from Definition 3.1. We also obtain

$$\begin{aligned} p_{i,\bar{x}} &= u_{i,\bar{x}x\bar{x}} - [\mathcal{Z}(u_i)]_{\bar{x}} \\ u_{i,\bar{x}x\bar{x}} &= \frac{u_{i+1} - 3u_i + 3u_{-1} - u_{i-2}}{\Delta x^3} = u^{(3)}_{i-\frac{1}{2}} + \alpha(x_{i-\frac{1}{2}})\Delta x^2 + O(\Delta x^4) \\ [\mathcal{Z}(u_i)]_{\bar{x}} &= \mathcal{Z}'(u_{i-\frac{1}{2}})\frac{u_i - u_{i-1}}{\Delta x} + \mathcal{Z}''(u_{i-\frac{1}{2}})\frac{(u_i - u_{i-\frac{1}{2}})^2 - (u_{i-1} - u_{i-\frac{1}{2}})^2}{2\Delta x} + O(\Delta x^2) + O(\Delta x^4) \\ &= \mathcal{Z}'(u_{i-\frac{1}{2}})\left[u'_{i-\frac{1}{2}} + \frac{\Delta x^2}{24}u^{(3)}_{i-\frac{1}{2}} + O(\Delta x^4)\right] + \mathcal{Z}''(u_{i-1/2})\left[\frac{\Delta x^2}{8}u'_{i-\frac{1}{2}}u''_{i-\frac{1}{2}} + O(\Delta x^4)\right]. \end{aligned}$$

After a simplification,

$$p_{i,\bar{x}} = u^{(3)}_{i-\frac{1}{2}} + \mathcal{Z}'(u_{i-\frac{1}{2}})u'_{i-\frac{1}{2}} + \gamma(x_{i-\frac{1}{2}})\Delta x^2 + O(\Delta x^4)$$

for some smooth function $\gamma(x)$. As a result,

$$\begin{aligned} [m(u_{i-1},u_i)(1+p_{i,\bar{x}})]_x &= \frac{1}{\Delta x}\left[m(u_i,u_{i+1})(1+p_{i+1,\bar{x}}) - m(u_{i-1},u_i)(1+p_{i,\bar{x}})\right] \\ &= \frac{1}{\Delta x}\left\{\mathcal{M}\left(\frac{u_i+u_{i+1}}{2}\right) + \beta\left(\frac{u_i+u_{i+1}}{2}\right)\left(\frac{u_{i+1}-u_i}{2}\right)^2 + O(\Delta x^3)\right\}\left\{1 + u^{(3)}_{i+\frac{1}{2}} + \mathcal{Z}'(u_{i+\frac{1}{2}})u'_{i+\frac{1}{2}} + \gamma(x_{i+\frac{1}{2}})\Delta x^2 + O(\Delta x^4)\right\} \\ &- \frac{1}{\Delta x}\left\{\mathcal{M}\left(\frac{u_i+u_{i-1}}{2}\right) + \beta\left(\frac{u_i+u_{i-1}}{2}\right)\left(\frac{u_{i-1}-u_i}{2}\right)^2 + O(\Delta x^3)\right\}\left\{1 + u^{(3)}_{i-\frac{1}{2}} + \mathcal{Z}'(u_{i-\frac{1}{2}})u'_{i-\frac{1}{2}} + \gamma(x_{i-\frac{1}{2}})\Delta x^2 + O(\Delta x^4)\right\}, \end{aligned}$$

Note that for any continuously differentiable function $g(s)$

$$\begin{aligned} g\left(\frac{u_i+u_{i+1}}{2}\right) &= g(u_{i+\frac{1}{2}}) + g'(u_{i+\frac{1}{2}})\frac{u''_{i+\frac{1}{2}}}{2}\left(\frac{\Delta x}{2}\right)^2 + O(\Delta x^4), \\ \left(\frac{u_{i+1}-u_i}{2}\right)^2 &= (u'_{i+\frac{1}{2}})^2\left(\frac{\Delta x}{2}\right)^2 + O(\Delta x^4). \end{aligned}$$

The above properties can be applied to $\mathcal{M}(s)$ and $\beta(s)$. Hence we conclude

$$[m(u_{i-1},u_i)(1+p_{i,\bar{x}})]_x = \left[\mathcal{M}(u_i)(1 + u^{(3)}_i - Z'(u_i)u'_i)\right]' + O(\Delta x^2).$$

□

5. Numerical Simulation

In this section, we illustrate the benefit of using the BEM over GM after comparing the performance of the two methods. Suppose we solve the problem (P) with

$$\mathcal{M}(h) = \frac{h^3\phi(\alpha h)}{3\phi(\alpha)},\ \phi(X) = \frac{3}{16X^3}[(1+X)^4(4\log(1+X)-3)+4(1+X)^2-1],$$
$$\mathcal{Z}_+(h) = -\frac{A_H}{h^3}, \quad \text{and} \quad \mathcal{Z}_-(h) = \frac{\alpha}{\eta(1+\alpha h)},$$

which corresponds to (FSM) in Ji et al.[18] with $\lambda = 0$. In their work, setting $\lambda = 0$ matched the experimental data better than setting $\lambda > 0$. Thus, this is a good example to demonstrate our method on. We assume the initial data to be

$$u_0(x) = 1.471(1 + 0.01 sin(\pi x/L)),\ L = 23.0,$$

with dimensionless parameters $\alpha = 10.6$, $\eta = 0.223227$, $A_H = 0.001$. The dimensionless parameters and the initial data are chosen to be in the range of the physical values.

The numerical schemes presented in Section 4 are continuous in time so we must discretize the time step for the implementation. We use θ-weighted time step with $\theta = \frac{1}{2}$ (semi-implicit).

Bounded Entropy Method (Semi-Implicit BEM)**.**

$$\begin{aligned}
&\left(1+\alpha\frac{u_i^{k+1}+u_i^k}{2}\right)\left(\frac{u_i^{k+1}-u_i^k}{\Delta t}\right)+[m(u_{i-1}^{k+1},u_i^{k+1})(1+p_{i,\bar{x}}^{k+1})]_x = 0, \quad p_i^{k+1} = u_{i,\bar{x}x}^{k+1} - \mathcal{Z}_+(u_i^{k+1}) - \mathcal{Z}_-(u_i^k)\\
&u_i(0) = u_0(i\Delta x),\ i = 0,1,2\cdots N\\
&m(s_1,s_2) = \begin{cases} \mathcal{M}(s_1) & s_1 = s_2 \\ (s_2-s_1)/\int_{s_1}^{s_2}\frac{1}{\mathcal{M}(s)}ds & s_1 \neq s_2 \end{cases}
\end{aligned} \tag{5}$$

While other terms involving spatial differences including $\mathcal{Z}_+$, are discretized implicitly, we point out that $\mathcal{Z}_-$ is discretized explicitly. Such discretization is a well-known technique that increases the stability of a numerical method by treating a concave term and a convex term separately [33, 38]. One may apply a fully implicit method, but this typically requires Δt to be very small. On the other hand, one can incorporate adaptive time stepping when applying the semi-implicit method. This concept will be discussed in depth in Section 5.2.We also note that one has to numerically calculate $\int_{s_1}^{s_2}\frac{1}{\mathcal{M}(s)}ds$ while evaluating $m(s_1,s_2)$. We used the Simpson's method with 2-4 grids to numerically integrate $1/\mathcal{M}(h)$ on $[u_{i-1},u_i]$.

We compare the above semi-implicit BEM to the fully implicit GM used in [18].

Generic Method (Implicit GM with average mobility)**.**

$$\begin{aligned}
&\left(1+\alpha\frac{u_i^{k+1}+u_i^k}{2}\right)\left(\frac{u_i^{k+1}-u_i^k}{\Delta t}\right)+[m(u_{i-1}^{k+1},u_i^{k+1})(1+p_{i,\bar{x}}^{k+1})]_x = 0, \quad p_i^{k+1} = u_{i,\bar{x}x}^{k+1} - \mathcal{Z}_+(u_i^{k+1}) - \mathcal{Z}_-(u_i^{k+1})\\
&u_i(0) = u_0(i\Delta x),\ i = 0,1,2\cdots N\\
&m(s_1,s_2) = \begin{cases} \mathcal{M}(s_1) & s_1 = s_2 \\ \mathcal{M}\left(\frac{u_i^{k+1}+u_i^k}{2}\right) & s_1 \neq s_2 \end{cases}
\end{aligned} \tag{6}$$

As mentioned previously, the method is fully implicit so Δt needs to be kept small. Thus, when we compare the performance of BEM with GM, we do not use adaptive time comparison. The calculation of $m(s_1,s_2)$ for GM is relatively simple since it does not require numerical integrations. We used Newton's iterations at each time step for both methods to solve discrete nonlinear equations. As long as Δt was kept small enough for each system, the iterations converged within 3-4 iterations. When the convergence was not quadratic, we decreased the Δt by 50%.

Figure 2 and Figure 3 show a comparison of numerical simulation results of the GM and the BEM methods. In Figure 2, one can observe a classic evolution of isolated droplets dynamic. The bigger droplet collides with a smaller one and merges into one droplet as the solution propagates. One can observe that the droplets merge earlier in GM than in BEM. GM cannot handle instability in an underresolved mesh setting, so the numerical solution results in a negative value. BEM maintains positivity after merging.

In figure 3, one can observe what happens at the singularity. At time $t = 1.6998$, GM coarse hits a negative value while BEM coarse and GM fine does not. One can see that the singularity affects the shape of the solution after the singularity point. We can see that BEM coarse still ensures the smoothness at near zero height of the solution. The singularity at the time prevents further numerical simulation from this time.

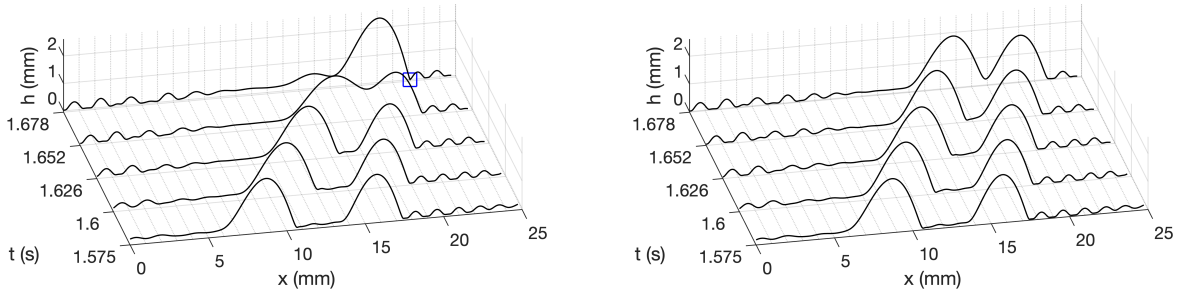

(a) GM (b) BEM

Fig. 2: PDE simulation results on a coarse grid using (a) Generic Method (GM) and (b) Bounded Entropy Method (BEM), illustrating the difference between the evolution profiles of the two methods when droplets merge. At $t = 1.652s$, GM prematurely fuses two droplets while BEM does not. As a result of this instability, GM develops negativity at $t = 1.678s$, indicated by the blue square marker. On the other hand, BEM can handle such instability and maintain the positivity of the film thickness.

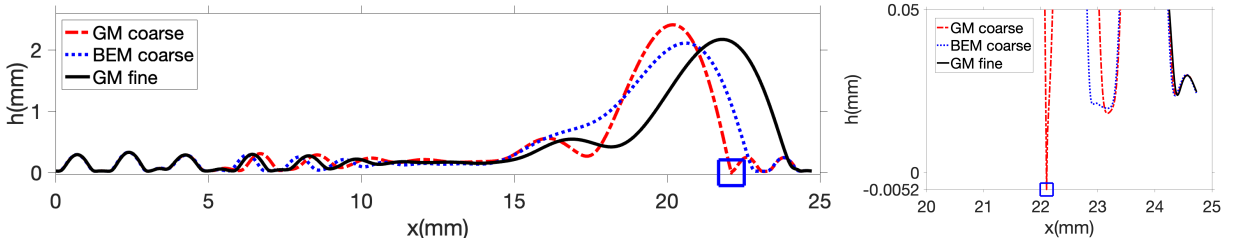

(a) Simulation comparison (b) Simulation comparison (enlarged)

Fig. 3: PDE simulation using Generic Method (GM) and Bounded Entropy Method (BEM), at the negativity $t = 1.6698s$. This is a snapshot of Figure 2 at $t = 1.6698s$. GM coarse and BEM coarse use 3072 points to discretize $[0, 24]$ which is equivalent resolution of discretizing $[0, 1]$ with 128 grid points. GM fine uses twice as many as grid points as the coarse grid for discretization following the standard presented in [47]. Besides the phase shift, BEM coarse agrees better with the GM fine despite the error caused by using different schemes.

5.1. Comparison with experiment

Figure 4 illustrates a schematic of experimental setup for the fiber coating. A programmable syringe pump introduces the liquid into the nozzle. Next to the coating flow, a high-speed camera was placed to operate at a frame rate of 1000 frame/second. A well-wetting liquid with low surface energy, Rhodorsil silicone oil v50 is used for the experiment. The detailed physical parameters are following: density $\rho = 963kg/m^3$, kinematic viscosity $\nu = 50mm^2/s$, surface tension $\sigma = 20.8mN/m$ at $20°C$ and capilary length $l_c = 1.5mm$. The flow rate of the liquid is carefully monitored by a weight scale connected to a computer so that it would range between $0.02g/s$ to $0.09g/s$. add a paragraph on experimental set up.

We consider two cases. In the first case, the flow rate is 0.08 g/s for a fiber radius of 0.1 mm with nozzle inner diameter ID = 0.8mm. This one corresponds to the Rayleigh-Plateau instability case. In another case, the flow rate is 0.04g/s for a fiber radius of 0.1mm with nozzle inner diameter ID = 1.8mm. This one corresponds to the Isolated Droplets regime.

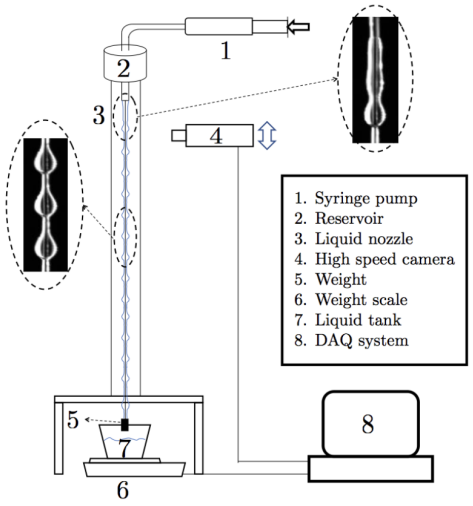

Fig. 4: Experimental setup. Same as the one used in [18].

The experimental data was extracted after image processing the high-quality resolution images. Such image analysis lets us calculate the nondimensional average thickness of $\bar{h}$ and period L. After finding $\bar{h}$ and L, we simulated BEM and GM with an initial data

$$u_0(x) = \bar{h}(1 + 0.01\sin(\pi x/L))$$

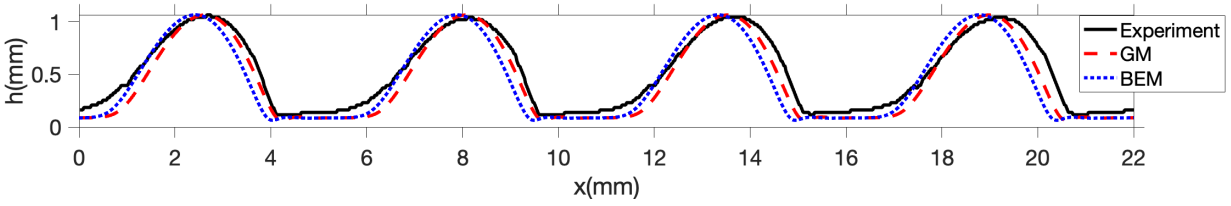

Fig. 5: Comparison between experimental data and the numerical methods. The experimental profile (the black solid line) follows the Rayleigh-Plateau regime, a flow rate of 0.08g/s, fiber radius of 0.1mm with nozzle ID = 0.8mm. GM and BEM were shifted horizontally to match the phase.

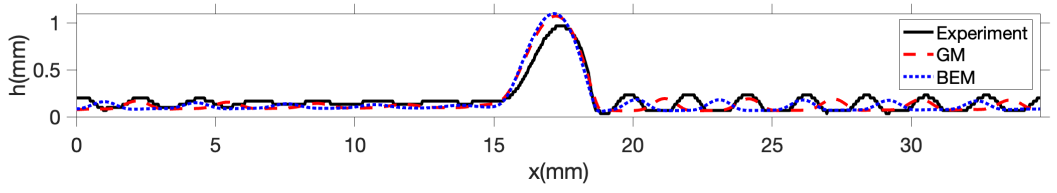

Fig. 6: Comparison between physical experimental data and the numerical methods. The experimental profile (the black solid line) follows the Isolated droplet regime, a flow rate is 0.04g/s, a fiber radius of 0.1mm with nozzle ID = 1.8mm. GM and BEM were shifted horizontally to match the phase. replace the photo so that the droplet is in the middle?

5.2. Adaptive time stepping

still need to finish writing The adaptive time step algorithm can optimize the performance of the numerical method while accurately capturing the droplet propagation [39, 64]. In the early stage of the computation, we expect to see a lot of change in the shape of the graph. Therefore, one wishes to keep the time step very small to capture the

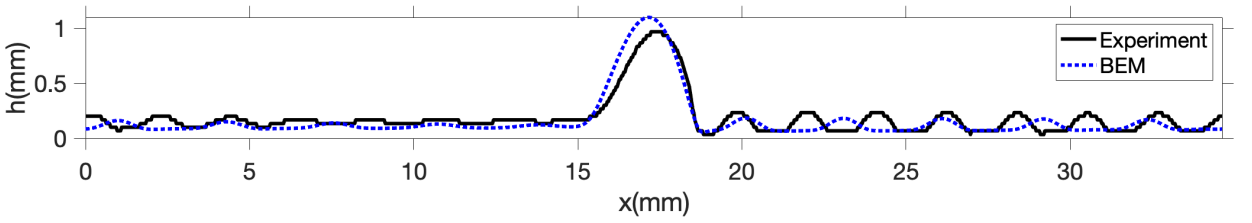

Fig. 7: Isolated Droplet Sample

accurate profile of the solution. However, as the computation progress, the algorithm approach a nearly steady state. It becomes costly to implement small time step calculation for many iterations while such small step iteration doesn't contribute much to the change of the profile or the phase. Here we use an adaptive time stepping scheme [64] for the efficiency of the computation.

We use a dimensionless local truncation error for every time step and see if it surpasses a tolerance value that we impose. The dimensionless local truncation error is calculated by the following formula.

$$LTE(t^{k+1}) = \left\| e^{k+1} - \frac{\Delta t}{\Delta t_{old}} e^{k} \right\|_{L^2}$$

We defined $e^{k+1} = \frac{u^{k+1}-u^k}{u^k}$ and $e^k = \frac{u^k-u^{k-1}}{u^{k-1}}$ whereas $\Delta t = t^{k+1} - t^k$ and $\Delta t_{old} = t^k - t^{k-1}$. Note that we have to store information of previous data u^{k-1} to calculate the error. After the calculation, if the error is less than tol_1,

Algorithm 1: Adaptive timestepping

Data: numerical solution u^{k-1}, u^k, u^{k+1}, the current time step Δt, the old time step Δt_{old}, adaptive time tolerance tol_1.
Result: the next time step Δt, previous time step Δt_{old}
while $t < t_{end}$ **do**
  if *newton's method succeed* **then**
    calculate $LTE(t^{k+1})$;
    $\Delta t_{old} = \Delta t$;
    if $LTE(t^{k+1}) < tol_1$ **then**
      $\Delta t = 1.1\Delta t$; /* Increase Δt by 10% */
    else
      $\Delta t = 1.01\Delta t$; /* Increase Δt by 1% */
    end
  else
    $\Delta t = 0.5\Delta t$; /* Try newton's method with 50% of Δt */
  end
end

Include a figure demonstrating adaptive time stepping

5.3. Computational Efficiency

still need to finish writing Given the following parameter setting, we calculated the CPU time of each method. We let $A_H = 0, \eta = 0.005, \alpha = 5.0$ with initial data

$$h_0(x) = 0.45 + 0.01\sin(\pi x), \text{ on } [0, 1]$$

	Positivity	l^2 error	CPU time (s)
GM with $\Delta x = 0.01$	fails	0.17	N/A
BEM $\Delta x = 0.01$	success	0.15	1.08
GM with $\Delta x = 0.0014$	success	0.12	1.296

6. Conclusion

In this paper, we introduce a positivity-preserving finite difference method for the problem fiber-coating a vertical cylindrical fiber. While the current state-of-the-art method (GM) achieves close agreement with experiments and successfully captures regime transitions, it struggles to match the flow profiles as the film thickness becomes small. In particular, the GM needs significant grid refinement to resolve a false premature rupture of the solution. We prove that our BEM preserves positivity given $\mathcal{M}(h) = O(h^n)$ for $n \geq 2$ and furthermore that there exists a lower bound independent of grid size given an a posteriori Lipschitz bound on the solution (something that is always observed in experiments). By constructing a generalized entropy estimate, we extend the idea of positivity-preserving methods for basic lubrication equations to the problem involving cylindrical geometry, gravity, and nonlinear pressure. This technique can potentially be used for thin liquid film equations with complex geometry, advection effect, and other surface tension effects.

There are a number of directions one can pursue from this work. One obvious direction is to examine the convergence of the BEM. Such work would benefit from additional theoretical results for the continuum PDE. Another direction is to generalize the method to the fully 2D fiber coating problem e.g. using ADI methods such as [65] or to consider more general geometries as in [66]. Finally, it would be interesting to consider other types of boundary conditions since the experiment is not done in a periodic geometry. The boundary conditions on an inlet and an outlet of the flow can change if other models are considered, such as one that includes a nozzle geometry [67] or a thermal effect [68].

Acknowledgments

This research is supported by the Simons Foundation Math + X Investigator Award number 510776. H.J. acknowledges support from Faculty Research and Professional Development Program (FRPD) provided by NC State University.

References

[1] D. Quéré, Thin films flowing on vertical fibers, EPL (Europhysics Letters) 13 (1990) 721.
[2] S. Kalliadasis, C. Ruyer-Quil, B. Scheid, M. G. Velarde, Falling liquid films, volume 176, Springer Science & Business Media, 2011.
[3] C. T. Gabbard, J. B. Bostwick, Asymmetric instability in thin-film flow down a fiber, Physical Review Fluids 6 (2021) 034005.
[4] K. Uchiyama, H. Migita, R. Ohmura, Y. H. Mori, Gas absorption into "string-of-beads" liquid flow with chemical reaction: application to carbon dioxide separation, International journal of heat and mass transfer 46 (2003) 457–468.
[5] J. Grünig, E. Lyagin, S. Horn, T. Skale, M. Kraume, Mass transfer characteristics of liquid films flowing down a vertical wire in a counter current gas flow, Chemical engineering science 69 (2012) 329–339.
[6] H. Chinju, K. Uchiyama, Y. H. Mori, "string-of-beads" flow of liquids on vertical wires for gas absorption, AIChE journal 46 (2000) 937–945.
[7] Z. Zeng, A. Sadeghpour, G. Warrier, Y. S. Ju, Experimental study of heat transfer between thin liquid films flowing down a vertical string in the rayleigh-plateau instability regime and a counterflowing gas stream, International Journal of Heat and Mass Transfer 108 (2017) 830–840.
[8] Z. Zeng, A. Sadeghpour, Y. S. Ju, Thermohydraulic characteristics of a multi-string direct-contact heat exchanger, International Journal of Heat and Mass Transfer 126 (2018) 536–544.
[9] T. Gilet, D. Terwagne, N. Vandewalle, Digital microfluidics on a wire, Applied physics letters 95 (2009) 014106.
[10] A. Sadeghpour, Z. Zeng, H. Ji, N. Dehdari Ebrahimi, A. Bertozzi, Y. Ju, Water vapor capturing using an array of traveling liquid beads for desalination and water treatment, Science advances 5 (2019) eaav7662.
[11] R. V. Craster, O. K. Matar, Dynamics and stability of thin liquid films, Reviews of modern physics 81 (2009) 1131.
[12] H.-C. Chang, E. A. Demekhin, Mechanism for drop formation on a coated vertical fibre, Journal of Fluid Mechanics 380 (1999) 233–255.
[13] C. Duprat, C. Ruyer-Quil, F. Giorgiutti-Dauphiné, Spatial evolution of a film flowing down a fiber, Physics of Fluids 21 (2009) 042109.
[14] C. Ruyer-Quil, P. Treveleyan, F. Giorgiutti-Dauphiné, C. Duprat, S. Kalliadasis, Modelling film flows down a fibre, Journal of Fluid Mechanics 603 (2008) 431–462.
[15] A. Sadeghpour, Z. Zeng, Y. S. Ju, Effects of nozzle geometry on the fluid dynamics of thin liquid films flowing down vertical strings in the rayleigh–plateau regime, Langmuir 33 (2017) 6292–6299.
[16] D. Quéré, Fluid coating on a fiber, Annual Review of Fluid Mechanics 31 (1999) 347–384.
[17] I. Kliakhandler, S. H. Davis, S. Bankoff, Viscous beads on vertical fibre, Journal of Fluid Mechanics 429 (2001) 381–390.
[18] H. Ji, C. Falcon, A. Sadeghpour, Z. Zeng, Y. Ju, A. Bertozzi, Dynamics of thin liquid films on vertical cylindrical fibres, Journal of Fluid Mechanics 865 (2019) 303–327.
[19] C. Ruyer-Quil, S. Trevelyan, F. Giorgiutti-Dauphiné, C. Duprat, S. Kalliadasis, Film flows down a fiber: Modeling and influence of streamwise viscous diffusion, The European Physical Journal Special Topics 166 (2009) 89–92.
[20] C. Ruyer-Quil, S. Kalliadasis, Wavy regimes of film flow down a fiber, Physical Review E 85 (2012) 046302.
[21] H. Ji, R. Taranets, M. Chugunova, On travelling wave solutions of a model of a liquid film flowing down a fibre, European Journal of Applied Mathematics (2021) 1–30.

[22] P. Li, Y. Chao, Marangoni instability of self-rewetting films modulated by chemical reactions flowing down a vertical fibre, Chemical Engineering Science 227 (2020) 115936.
[23] A. Frenkel, Nonlinear theory of strongly undulating thin films flowing down vertical cylinders, EPL (Europhysics Letters) 18 (1992) 583.
[24] R. Craster, O. Matar, On viscous beads flowing down a vertical fibre, Journal of Fluid Mechanics 553 (2006) 85–105.
[25] D. Halpern, H.-H. Wei, Slip-enhanced drop formation in a liquid falling down a vertical fibre, Journal of Fluid Mechanics 820 (2017) 42–60.
[26] Y. Y. Trifonov, Steady-state traveling waves on the surface of a viscous liquid film falling down on vertical wires and tubes, AIChE journal 38 (1992) 821–834.
[27] G. M. Sisoev, R. V. Craster, O. K. Matar, S. V. Gerasimov, Film flow down a fibre at moderate flow rates, Chemical engineering science 61 (2006) 7279–7298.
[28] E. Novbari, A. Oron, Energy integral method model for the nonlinear dynamics of an axisymmetric thin liquid film falling on a vertical cylinder, Physics of Fluids 21 (2009) 062107.
[29] C. Duprat, C. Ruyer-Quil, S. Kalliadasis, F. Giorgiutti-Dauphiné, Absolute and convective instabilities of a viscous film flowing down a vertical fiber, Physical review letters 98 (2007) 244502.
[30] L. B. Smolka, J. North, B. K. Guerra, Dynamics of free surface perturbations along an annular viscous film, Physical Review E 77 (2008) 036301.
[31] B. Reisfeld, S. Bankoff, Non-isothermal flow of a liquid film on a horizontal cylinder, Journal of Fluid Mechanics 236 (1992) 167–196.
[32] D. Bonn, J. Eggers, J. Indekeu, J. Meunier, E. Rolley, Wetting and spreading, Reviews of modern physics 81 (2009) 739.
[33] G. Grün, M. Rumpf, Simulation of singularities and instabilities arising in thin film flow, European Journal of Applied Mathematics 12 (2001) 293–320.
[34] A. Oron, S. H. Davis, S. G. Bankoff, Long-scale evolution of thin liquid films, Reviews of modern physics 69 (1997) 931.
[35] J. Becker, G. Grün, R. Seemann, H. Mantz, K. Jacobs, K. R. Mecke, R. Blossey, Complex dewetting scenarios captured by thin-film models, Nature materials 2 (2003) 59–63.
[36] H.-W. Lu, K. Glasner, A. Bertozzi, C.-J. Kim, A diffuse-interface model for electrowetting drops in a hele-shaw cell, Journal of Fluid Mechanics 590 (2007) 411–435.
[37] K. Maki, R. Braun, P. Ucciferro, W. Henshaw, P. King-Smith, Tear film dynamics on an eye-shaped domain. part 2. flux boundary conditions, Journal of fluid mechanics 647 (2010) 361–390.
[38] G. Grün, On the convergence of entropy consistent schemes for lubrication type equations in multiple space dimensions, Mathematics of computation 72 (2003) 1251–1279.
[39] A. L. Bertozzi, M. P. Brenner, T. F. Dupont, L. P. Kadanoff, Singularities and similarities in interface flows, in: Trends and perspectives in applied mathematics, Springer, 1994, pp. 155–208.
[40] A. L. Bertozzi, Symmetric singularity formation in lubrication-type equations for interface motion, SIAM Journal on Applied Mathematics 56 (1996) 681–714.
[41] L. Yu, J. Hinch, The velocity of 'large'viscous drops falling on a coated vertical fibre, Journal of fluid mechanics 737 (2013) 232–248.
[42] X. Zhang, C.-W. Shu, On positivity-preserving high order discontinuous galerkin schemes for compressible euler equations on rectangular meshes, Journal of Computational Physics 229 (2010) 8918–8934.
[43] X. Zhang, C.-W. Shu, Maximum-principle-satisfying and positivity-preserving high-order schemes for conservation laws: survey and new developments, Proceedings of the Royal Society A: Mathematical, Physical and Engineering Sciences 467 (2011) 2752–2776.
[44] J. Droniou, C. L. Potier, Construction and convergence study of schemes preserving the elliptic local maximum principle, SIAM journal on numerical analysis 49 (2011) 459–490.
[45] Q. Du, L. Ju, X. Li, Z. Qiao, Maximum bound principles for a class of semilinear parabolic equations and exponential time-differencing schemes, SIAM Review 63 (2021) 317–359.
[46] J. W. Barrett, J. F. Blowey, H. Garcke, Finite element approximation of a fourth order nonlinear degenerate parabolic equation, Numerische Mathematik 80 (1998) 525–556.
[47] L. Zhornitskaya, A. L. Bertozzi, Positivity-preserving numerical schemes for lubrication-type equations, SIAM Journal on Numerical Analysis 37 (1999) 523–555.
[48] G. Grün, M. Rumpf, Nonnegativity preserving convergent schemes for the thin film equation, Numerische Mathematik 87 (2000) 113–152.
[49] B. Li, J. Yang, Z. Zhou, Arbitrarily high-order exponential cut-off methods for preserving maximum principle of parabolic equations, SIAM Journal on Scientific Computing 42 (2020) A3957–A3978.
[50] C. Lu, W. Huang, E. S. Van Vleck, The cutoff method for the numerical computation of nonnegative solutions of parabolic pdes with application to anisotropic diffusion and lubrication-type equations, Journal of Computational Physics 242 (2013) 24–36.
[51] W. Chen, C. Wang, X. Wang, S. M. Wise, Positivity-preserving, energy stable numerical schemes for the cahn-hilliard equation with logarithmic potential, Journal of Computational Physics: X 3 (2019) 100031.
[52] L. Dong, C. Wang, H. Zhang, Z. Zhang, A positivity-preserving, energy stable and convergent numerical scheme for the cahn–hilliard equation with a flory–huggins–degennes energy, Communications in Mathematical Sciences 17 (2019) 921–939.
[53] J. Hu, X. Huang, A fully discrete positivity-preserving and energy-dissipative finite difference scheme for poisson–nernst–planck equations, Numerische Mathematik 145 (2020) 77–115.
[54] D. J. Eyre, Unconditionally gradient stable time marching the cahn-hilliard equation, MRS Online Proceedings Library (OPL) 529 (1998).
[55] B. P. Vollmayr-Lee, A. D. Rutenberg, Fast and accurate coarsening simulation with an unconditionally stable time step, Physical Review E 68 (2003) 066703.
[56] F. Huang, J. Shen, K. Wu, Bound/positivity preserving and unconditionally stable schemes for a class of fourth order nonlinear equations, Journal of Computational Physics 460 (2022) 111177.
[57] F. Bernis, A. Friedman, Higher order nonlinear degenerate parabolic equations, Journal of differential equations 83 (1990) 179–206.
[58] A. L. Bertozzi, M. Pugh, The lubrication approximation for thin viscous films: the moving contact line with a'porous media'cut-off of van der waals interactions, Nonlinearity 7 (1994) 1535.
[59] V. A. Solonnikov, On boundary value problems for linear parabolic systems of differential equations of general form, Trudy Matematicheskogo Instituta Imeni VA Steklova 83 (1965) 3–163.
[60] D. Desbrow, S. d. eidel'man, parabolic systems (north-holland, wolters-nordhoff, 1969), v 469pp., £7·60., Proceedings of the Edinburgh

Mathematical Society 17 (1971) 371–371.
[61] A. FRIEDMAN, Interior estimates for parabolic systems of partial differential equations, Journal of Mathematics and Mechanics 7 (1958) 393–417.
[62] A. L. Bertozzi, M. Pugh, The lubrication approximation for thin viscous films: Regularity and long-time behavior of weak solutions, Communications on pure and applied mathematics 49 (1996) 85–123.
[63] R. J. LeVeque, R. J. Leveque, Numerical methods for conservation laws, volume 214, Springer, 1992.
[64] T. Kostić, A. Bertozzi, Statistical density estimation using threshold dynamics for geometric motion, Journal of Scientific Computing 54 (2013) 513–530.
[65] T. P. Witelski, M. Bowen, Adi schemes for higher-order nonlinear diffusion equations, Applied Numerical Mathematics 45 (2003) 331–351.
[66] J. B. Greer, A. L. Bertozzi, G. Sapiro, Fourth order partial differential equations on general geometries, Journal of Computational Physics 216 (2006) 216–246.
[67] H. Ji, A. Sadeghpour, Y. S. Ju, A. L. Bertozzi, Modelling film flows down a fibre influenced by nozzle geometry, Journal of Fluid Mechanics 901 (2020).
[68] H. Ji, C. Falcon, E. Sedighi, A. Sadeghpour, Y. S. Ju, A. L. Bertozzi, Thermally-driven coalescence in thin liquid film flowing down a fibre, Journal of Fluid Mechanics 916 (2021).